AGU ADVANCING EARTH AND SPACE SCIENCES

Geophysical Research Letters

RESEARCH LETTER
10.1029/2025GL116865

The Substorms of 26 February 2008: A Data-Mining Perspective

M. I. Sitnov[1], G. K. Stephens[1], T. Motoba[1], and N. A. Tsyganenko[2]

[1]The Johns Hopkins University Applied Physics Laboratory, Laurel, MD, USA, [2]Saint-Petersburg State University, Saint-Petersburg, Russia

Key Points:

- Data mining technology resolves the X-line suggested earlier by multi-probe observations and it also detects current disruption signatures
- The most prominent feature of substorm activations is the rapid earthward redistribution of magnetic flux in the premidnight sector
- Comparison of low-altitude mapping of the magnetotail with all-sky imager data points to the likely location of the substorm trigger

Supporting Information:

Supporting Information may be found in the online version of this article.

Correspondence to:

M. I. Sitnov,
Mikhail.Sitnov@jhuapl.edu

Citation:

Sitnov, M. I., Stephens, G. K., Motoba, T., & Tsyganenko, N. A. (2025). The substorms of 26 February 2008: A data-mining perspective. *Geophysical Research Letters*, *52*, e2025GL116865. https://doi.org/10.1029/2025GL116865

Received 5 MAY 2025
Accepted 3 OCT 2025

Author Contributions:

Conceptualization: M. I. Sitnov
Data curation: M. I. Sitnov, T. Motoba
Formal analysis: M. I. Sitnov
Funding acquisition: M. I. Sitnov
Investigation: M. I. Sitnov, G. K. Stephens, T. Motoba, N. A. Tsyganenko
Methodology: M. I. Sitnov, G. K. Stephens, T. Motoba, N. A. Tsyganenko
Project administration: M. I. Sitnov
Resources: M. I. Sitnov
Software: G. K. Stephens, T. Motoba
Supervision: M. I. Sitnov
Validation: M. I. Sitnov, G. K. Stephens, T. Motoba
Visualization: M. I. Sitnov, G. K. Stephens

Abstract Reconstruction of the magnetospheric magnetic field using swarms of virtual spacecraft provided by data mining confirms seminal in situ evidence (Angelopoulos et al., 2008, https://doi.org/10.1126/science.1160495) that on 26 February 2008 an X-line emerged in the region between two distant Time History of Events and Macroscale Interactions during Substorms probes at the time of the substorm activation in the magnetotail. It also shows that the X-line formation was preceded by rapid current decay that happened 15 min earlier. The current was built up earthward of the pre-existing X-line formed prior to the previous substorm activation 45 min before. The most pronounced effect of the tail reconfiguration at the moments of two substorm activations and the current disruption is the rapid earthward redistribution of the magnetic flux. Comparison of low-altitude mapping of the magnetotail structure with all-sky imager data shows that these rapid reconfigurations might be triggered by plasma flows whose source was farther from the Earth than the resolved X-lines.

Plain Language Summary One of the most discussed findings of the five-probe Time History of Events and Macroscale Interactions during Substorms mission has become the detection of signatures of magnetic reconnection made on 26 February 2008 by the two probes farthest from the Earth. However, those signatures, critically important for understanding the role of reconnection and non-reconnection processes in magnetospheric substorms, were rather unconventional and local. And they couldn't be verified by other observations or global empirical models. Here we show that modern machine-learning techniques can support the original local observations and enrich the substorm description due to the detailed empirical reconstruction of the magnetic field extracted from historical data archives for similar events.

1. Introduction

Seventeen years ago Angelopoulos et al. (2008) (hereafter AN08) published a paper, aimed to finally resolve the substorm trigger dilemma: Are substorms triggered by the disruption of the electric current flowing across the near-Earth magnetotail, at ∼10 R_E (R_E = 6371.2 km is Earth's radius) or by magnetic reconnection (MR) at larger downtail distances ∼20 to 30 R_E? The Time History of Events and Macroscale Interactions during Substorms (THEMIS) mission (Angelopoulos, 2008), designed to solve this problem, consisted of five probes distributed along the tail to detect the near-Earth current disruption (CD) signatures and to locate X-lines associated with MR. The results of observations of the 26 February 2008 substorm reported in AN08 favored the reconnection trigger scenario, although discussions about the generality of these results and their details are still ongoing (Angelopoulos et al., 2009; Lui, 2009, 2020; Stephens et al., 2023). These debates were caused by both the uniqueness of the substorm onset at 04:55–05:00 UT of 26 February 2008, with all five THEMIS probes distributed along the tail from ∼7 to ∼21 R_E, and the details of the reconnection process detection, which were rather unconventional and limited in magnetic local time (MLT). In particular, the first sign of reconnection was the plasma motion toward the neutral sheet, rather than divergent (tailward/earthward) outflows.

In this study we analyze the substorm onset addressed in AN08 (hereafter SO2) and an earlier onset (SO1) at 04:05 UT (Angelopoulos et al., 2009; Lui, 2009; Pu et al., 2010), using another approach based on AI technology. While the ongoing debates regarding the priority of MR (Baker et al., 1996) or CD (Lui, 1996) scenarios remain the background of our analysis, its goal is rather to draw a global picture and evolution of the magnetic field and electric currents during these substorms in space, as well as at low altitudes where it may be compared with all-sky imager (ASI) data (Mende et al., 2008), the problems beyond the reach of classic empirical geomagnetic field models like T96 (Tsyganenko, 1995, 1996; Tsyganenko & Stern, 1996). In spite of the fact that our

Writing – original draft: M. I. Sitnov
Writing – review & editing: G. K. Stephens, T. Motoba, N. A. Tsyganenko

reconstructions remain limited to the magnetostatic approximation and, hence, time scales $\gtrsim$5 min (the time of the Alfvén wave propagation across the magnetosphere), the resulting picture nicely complements previous multi-probe observations and helps better understand the underlying physical processes and their causality.

One of the biggest problems in the definitive answer to the substorm causality question is the extreme paucity of space observations. The five-probe THEMIS mission remains so far the largest constellation of probes, which may at best be doubled in lucky cases when other mission probes are located close to the region of interest (e.g., Angelopoulos et al., 2013; Turner et al., 2017). Meanwhile, instead of using very limited sets of concurrent observations or statistical approaches, trying to fit all the real-world complexities into a simple analytical model, one can use the recurring nature of storms and substorms to complement the real observations by synthetic data. The synthetic set is a small subset of the historical database formed by observations, which surround the event of interest in the space of global activity parameters, quantified by geomagnetic indices, *SMR* for storms and *SML* for substorms (Gjerloev, 2012), as well as the solar wind electric field vB_z^{IMF} (v is the solar wind speed and B_z^{IMF} is the z-component of the interplanetary magnetic field (IMF) in the Geocentric Solar Magnetic coordinate system used hereafter), which quantify the solar wind/IMF driving. In the modern machine-learning (ML) nomenclature, such an approach, when at every instance the new empirical description of the system is formed, is called *instance-based* learning (e.g., Dou et al., 2023) to contrast it with the *model-based* learning when a single universal model, like T96, is created for all instances. This approach, also known as data mining (DM) (Aggarwal, 2014; Sun & Chen, 2021) using the nearest-neighbor method (Cover & Hart, 1967) has been developed with applications to magnetospheric storms and substorms in (Sitnov et al., 2008; Stephens et al., 2019) following (Vassiliadis, 2006; Vassiliadis et al., 1995) rooted in the general prediction/modeling using local approximations (Farmer & Sidorowich, 1987).

The DM approach is advantageous over conventional statistical modeling in that it is sensitive to different phases and activity levels of storms and substorms. On the other hand, since the number of the nearest neighbors (NNs) in the specific subset may greatly exceed the number of real probes, it allows one to use far more complex and flexible magnetic field architectures (Stephens et al., 2019; Tsyganenko & Sitnov, 2007), which resolve, in particular, the location of individual X-lines (Stephens et al., 2023). The large number of NNs also gives the reconstructions of the individual events statistical significance, suggesting that the effect under scrutiny, such as, for instance, an X-line bracketed by probes P1 and P2 in AN08, reflects the general feature of the system. Being event-oriented, the DM approach is still drastically different from conventional event-oriented adapted models (AMs) (e.g., Kubyshkina et al., 2009, and refs. therein) where a statistical model, like T96, is reinforced (for instance, to describe an additional thin current sheet module important for substorms) and then tuned to match a few real observations or isotropic precipitation boundaries (IBs). Having much fewer degrees of freedom, AMs are limited in their reconstructions to lucky cases with sufficient numbers of real probes during the event of interest. They are also limited in space to the immediate vicinities of the real probe location or the IB source region, beyond which the AMs perform no better than their base statistical model.

Here we show how DM helps provide a detailed empirical reconstruction of the magnetic field during the 26 February 2008 substorms. It supports the original local observations and enriches the substorm evolution picture with interesting implications for the substorm mechanism.

2. Details of Data Mining and Magnetic Field Architecture

Since the main details of the DM algorithm have already been reported earlier (Shi et al., 2024; Sitnov et al., 2008; Stephens et al., 2019; Stephens & Sitnov, 2021; Tsyganenko & Sitnov, 2007), here we only briefly describe the key elements and distinctive features of the specific version used here, while the complete description is provided in the Supporting Information S1.

In the DM approach, for every moment of interest we search for a small ($\sim$0.25%) NN subset of the database formed from 10,406,381 magnetometer records, mainly with 5-min cadence, provided by the Geotail, THEMIS/ARTEMIS, Van Allen Probes, Cluster II, Polar, IMP-8, GOES 8, 9, 10, 12 and MMS missions. The search (mining proper) is made by selecting the events closest to the event of interest in the 6-D space of global parameters G_1-G_6 formed by geomagnetic indices *SMR* and *SML*, their time derivatives, as well as the solar wind and IMF parameters vB_s^{IMF} ($B_s^{IMF} = -B_z^{IMF}$ when $B_z^{IMF} < 0$ and $B_s^{IMF} = 0$ otherwise) and B_y^{IMF}, averaged over storm and substorm scales and sampled with a 5-min cadence. Based on our previous studies (Sitnov et al., 2019), we choose the subsets

of $32 \cdot 10^3$ moments, which corresponds to $\sim 10^5$ magnetometer records per subset. However, since the NNs are additionally weighted in the fitting procedure, as is specified in Supporting Information S1, the effective number of virtual spacecraft observations employed for reconstruction at every moment is $\sim 26,000$.

The large number of these virtual spacecraft picked by DM at every moment allows one to use a very flexible architecture for the magnetic field (Shi et al., 2024; Stephens et al., 2019, 2023) to fit the NN subset. It includes two independent representations of thick and thin tail current sheets by $(2M + 1) \times N$ basis function expansions with M azimuthal and N radial basis functions and data-derived thickness parameters D and D_{TCS}, respectively (TCS stands for "thin current sheet"). A similar basis function representation is used for the field-aligned current (FAC) system. The base model architecture, called ARGUS, is available online at (Stephens et al., 2024). The whole magnetic field model configuration includes 1,056 linear amplitude coefficients (1,040 for equatorial and 16 for FAC expansions) and 10 non-linear parameters describing thick and thin current sheet parameters, hinging, warping and twisting parameters, as well as FAC scaling parameters detailed in Supporting Information S1. The model field is additionally deformed to take into account the tilt angle variations (Stephens et al., 2023; Tsyganenko & Andreeva, 2014).

Two important adjustments have been introduced in this study, compared to the base DM algorithm and ARGUS architecture. First, to mitigate the relatively short duration of the substorm activations in this event, we reduced the averaging scale for substorm binning parameters (Equations 3 and 4 in Supporting Information S1) to $\Pi_{\text{sst}} = 1$ h, corresponding to $\sim$15-min average in time, compared to $\sim$30-min scale used in earlier studies and consistent with average substorm scales (e.g., Partamies et al., 2013). Second, to mitigate the problem of the $\gtrsim 1°$ uncertainty of most empirical geomagnetic field models in their mapping to low altitudes (Nishimura et al., 2011; Shevchenko et al., 2010), critical for the prebreakup arc mapping (V. Sergeev et al., 2012), we applied the merged resolution method (Stephens & Sitnov, 2021) detailed in Supporting Information S1. As it has been recently shown (Shi et al., 2024), this method solves the mapping uncertainty problem and reveals that its likely cause is the underresolved transition region between the tail and the inner magnetosphere.

3. X-Lines and Current Disruption Signatures

We start the description of DM reconstructions from validation results for probes P1–P5 presented in Figure S1 in Supporting Information S1. Panels (e) and (f) in these plots show that the event indeed consisted of two substorm onsets, SO1 and SO2 at around 04:05 and 04:55 UT, respectively. The former was preceded by a conventional growth phase with $-vB_z^{IMF} = 0.5 - 1$ mV/m. The interval between SO1 and SO2 was a combination of the recovery phase for SO1 (04:10–04:45 UT) and the short growth phase for SO2 (04:45–05:00 UT). Note that, for consistency with our previous substorm reconstructions (e.g., Stephens et al., 2019), we define the onset of the expansion phase by the rapid decrease of the substorm index *SML*. This definition differs from that in AN08, 04:54 UT, based on the initial slow increase of their THEMIS *AE* index, but it shouldn't affect the subsequent analysis. The validation plots show that our reconstructions capture dipolarizations (B_z increases) in the near-Earth tail during both onsets SO1 and SO2, recorded by probes P3 and P4. They also show that the growth phase before the onsets is reproduced fairly well ($\delta B_z \lesssim 1$ nT) for all but one (P4) probes. Smaller amplitudes of SO1 and SO2 onsets, compared to observations, are likely caused by delays between near-Earth dipolarizations and the auroral electrojet as well as the residual 15-min time averaging of the *SML* index in the binning procedure, whose effect can be seen in Figure S2c in Supporting Information S1. Figure S2 in Supporting Information S1, comparing the original binning parameters G_1-G_6 with their averages over NN bins, confirms that, in spite of the unavoidable smoothing effects, NNs closely follow the evolution of these substorms in the binning space.

The onset of reconnection during SO2 had been inferred by AN08 indirectly, from their observations of the equatorward motion of plasma at 04:50 UT detected by probes P1 and P2, accompanied by small, negative at P1 and positive at P2, excursions of the B_z field. These indirect and rather subtle signatures later became the points of criticism and subsequent debates (Angelopoulos et al., 2009; Lui, 2009). Meanwhile, Figure 1 in AN08 showing an X-line between P1 and P2 was only an artist rendition, because the applied magnetic field model, T96, did not reveal any X-line during this event. In fact, it was simply unable to do so, because the tail current module in T96 is limited to only two custom-made current blocks, as described in more detail in (Tsyganenko, 2002). Thus, the topology change, which can only be provided by the local pinching of the tail current, could not be reproduced.

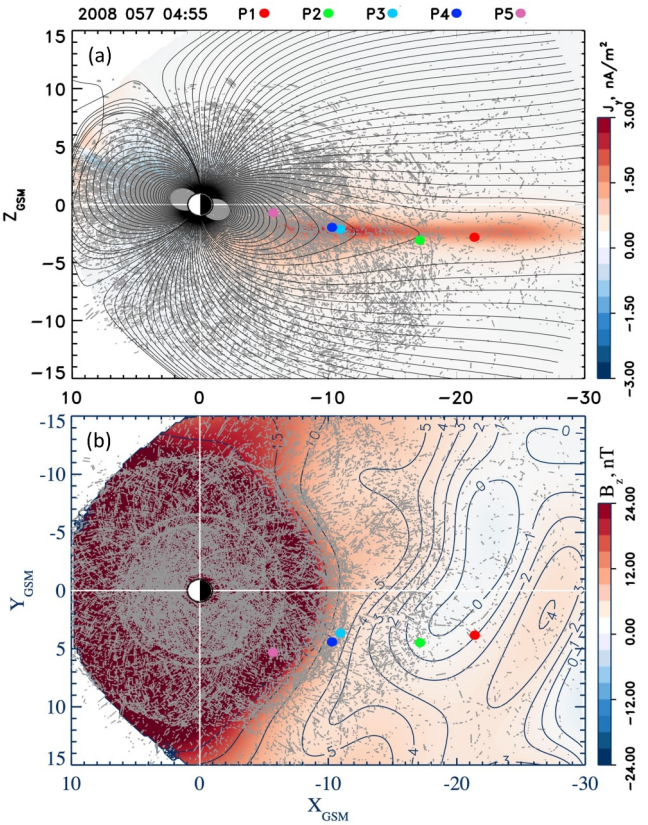

Figure 1. The magnetic field configuration near the SO2 onset (04:55 UT): (a) Color-coded distribution of the current density $J_y(x,z)$ in the midnight meridional plane with overplotted magnetic field lines (black lines) and $L_{NN} = 103,865$ virtual spacecraft observations used to reconstruct the magnetic field at this time (gray dots), including color-coded Time History of Events and Macroscale Interactions during Substorms probes P1–P5; (b) equatorial distribution of the magnetic field B_z (with zero geodipole tilt to simplify the visualization) and the corresponding projections of the nearest neighbors. The X-line near probes P1 and P2 is the earthward part of the $B_z = 0$ iso-contour. It is an earthward part of the plasmoid, to be further discussed in Section 5 (Figure 4c).

Now Figure 1b shows such an X-line. Moreover, its suggests that it is a generic feature of this specific state of the magnetosphere determined by the global binning parameters (Equations 1–6 in Supporting Information S1) and reconstructed using ∼26,000 virtual spacecraft observations, representing ∼0.25% of our database. Therefore, on the one hand, this reconstruction is strongly event-oriented, and on the other hand, it has a strong statistical significance, making it different from a simple assimilation of five THEMIS probes available at the moment of interest. Thus, Figure 1 confirms the original interpretation made in AN08 that probes P1 and P2 framed an X-line near SO2.

In order to guide subsequent analysis we provide in Figure S3 in Supporting Information S1 a summary of our reconstructions in a form similar to (Sitnov et al., 2019). In particular, Figure S3d in Supporting Information S1 shows that the expansion phases after SO1 and SO2 are marked by the increase of the low-latitude FAC intensity (FAC R2), with the latter being preceded by two high-latitude current (FAC R1) increases at 04:45 and 05:00 UT (Figure S3c in Supporting Information S1).

Figure S3g in Supporting Information S1 shows that both onsets are also marked by the increase of the B_z field at 12 R_E. According to Figure S3h in Supporting Information S1, for SO1, it started at 04:00 in the radial range 12–18 R_E (gray arrow pointing up), 5 min before the index onset SO1. The further dipolarization and brief recovery are seen in Figure S3i in Supporting Information S1 and highlighted there by gray arrows pointing up and down. Figures S3i and S3j in Supporting Information S1 suggest that after SO1 the tail was stretched again (the gray arrows pointing down), likely in the form of the flux redistribution within the closed field line region. The second dipolarization is marked by the gray arrow in Figure S3k in Supporting Information S1, although, according to Figure S3g in Supporting Information S1, around SO2, it is more complex compared to SO1, with two B_z increases after 04:45 and 05:00 UT. The comparison of the midnight B_z profiles provided in Figures S3h–S3k in Supporting Information S1 with similar profiles of substorms studied before (Sitnov et al., 2019; Sitnov, Stephens, et al., 2021; Stephens et al., 2019, 2023) suggests that the pre-onset equatorial magnetic field in the radial range 15–25 R_E was particularly small with $B_z \approx 1 - 2$ nT making the TCS prone to MR (tearing (Coppi et al., 1966; Schindler, 1974)) and CD (current-driven (Lui et al., 1990)) instabilities.

As is seen from Figure S3f in Supporting Information S1, the TCS strength reaches its maximum at 04:45 UT and then it rapidly drops, well before the SO2 onset, defined either by the substorm indices (e.g., Figure S3b in Supporting Information S1) or by local observations (04:50, according to Table 1 in AN08). This is confirmed by Figures 2a–2d and 2i–2l showing the evolution of the total equatorial and meridional current density distributions. The resulting disruption of the equatorial current and its deviation toward the ionosphere, similar to its original concept (Crooker & McPherron, 1972; McPherron et al., 1973), is also shown in Figure S4 in Supporting Information S1 in the format of (Stephens et al., 2019, Figure 10). It may indeed be explained by the corresponding current instability (Lui et al., 1990). However, for these relatively weak substorms, the peak current density $J_y \approx 3$ nA/m^2 was rather small compared to $J_y \approx 10$ nA/m^2 for stronger substorms in (Sitnov et al., 2019), while the TCS thickness was relatively large ($D_{TCS} \sim 1\ R_E$, according to Figure S3e in Supporting Information S1; see also the detailed profiles of $D_{TCS}(\rho)$ in Figure S5 in Supporting Information S1) compared to the Speiser (1965) orbit scale ∼0.2 R_E corresponding to unmagnetized ions and required for CD instabilities (Lui et al., 1990). Note that the CD onset is identified here as a plasma physics phenomenon based solely on the reconstructed buildup and decay of the tail current. In particular, it does not have the corresponding substorm manifestations in *SML* index. Moreover, the current increase prior to CD was accompanied by X-line formed tailward of 22 R_E and shown in Figure 2f. However, one cannot claim that the formation of the latter is a cause of the CD. This X-line

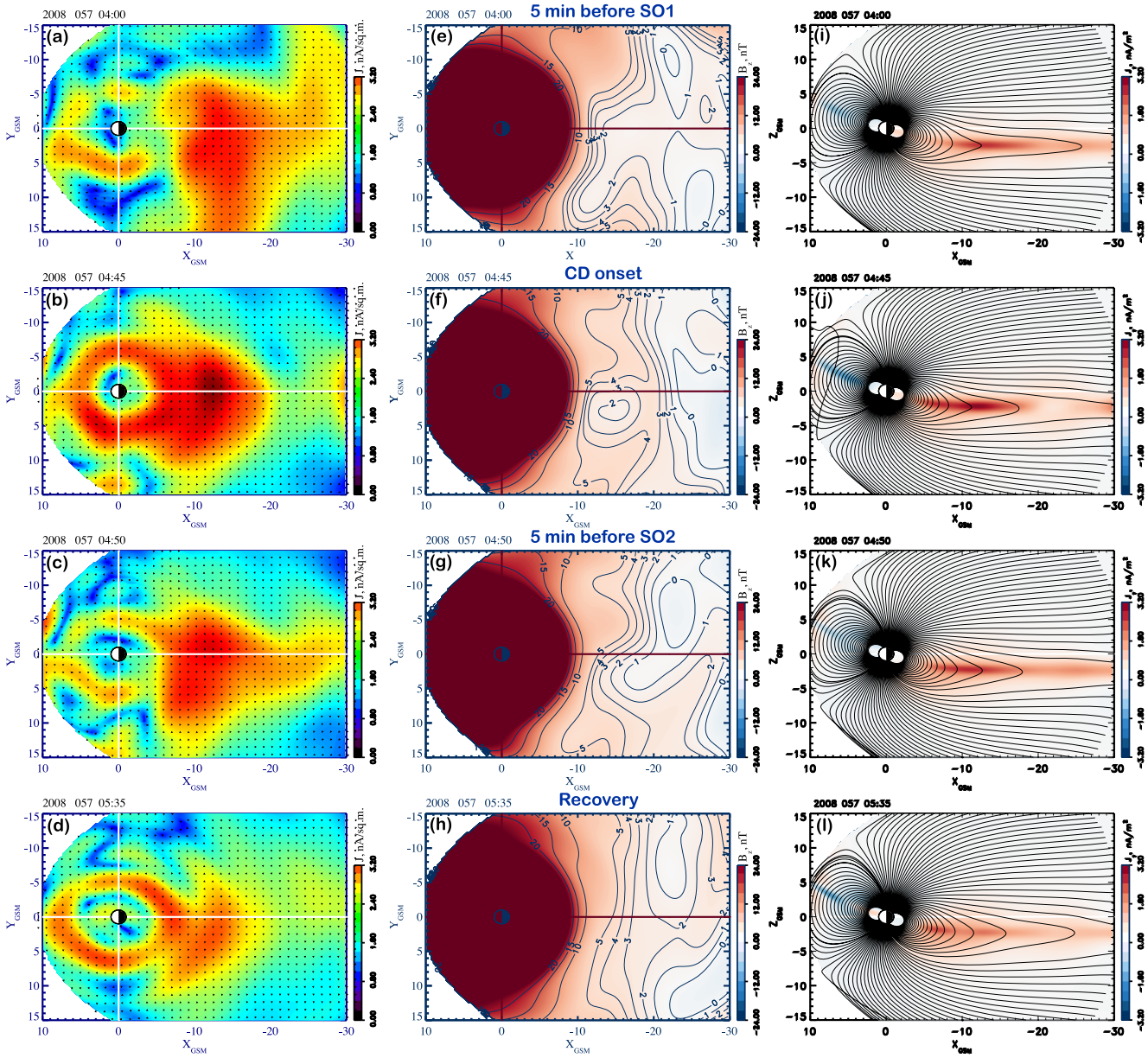

Figure 2. (a–d) The color-coded equatorial distributions of the current density $J = \sqrt{J_x^2 + J_y^2}$ (the arrows display the equatorial current vectors) and (e–h) the magnetic field B_z (with zero dipole tilt angle, for simplicity); (i–l) midnight meridional distributions of the current density J_y with sample field lines starting in the ionosphere from 50° with 1° step in latitude near onsets SO1, SO2, current disruption and in the recovery phase.

appears in the pre-midnight sector already in the growth phase of SO1 and only somewhat changes its shape during the whole event remaining largely outside 20 R_E (Figures 2e–2h). It shows the complexity of "substorm sequence" and its dependence on prehistory.

4. Magnetic Flux Redistribution

To reveal the process that most clearly distinguishes SO1, SO2, and CD onsets, we present in Figure 3 distributions of the equatorial field variations $dB_z = B_z(t_{i+1}) - B_z(t_i)$, where t_i is the time series in our reconstructions. Beyond the tail hinging distance or for small tilt angles, the B_z component dominates the magnetic field in the equatorial plane and therefore its distribution is the best measure of the magnetic flux. Figure 3 clearly shows three intervals of rapid flux redistribution (Figures 3e, 3h and 3k) on the time scale of 5 min, associated

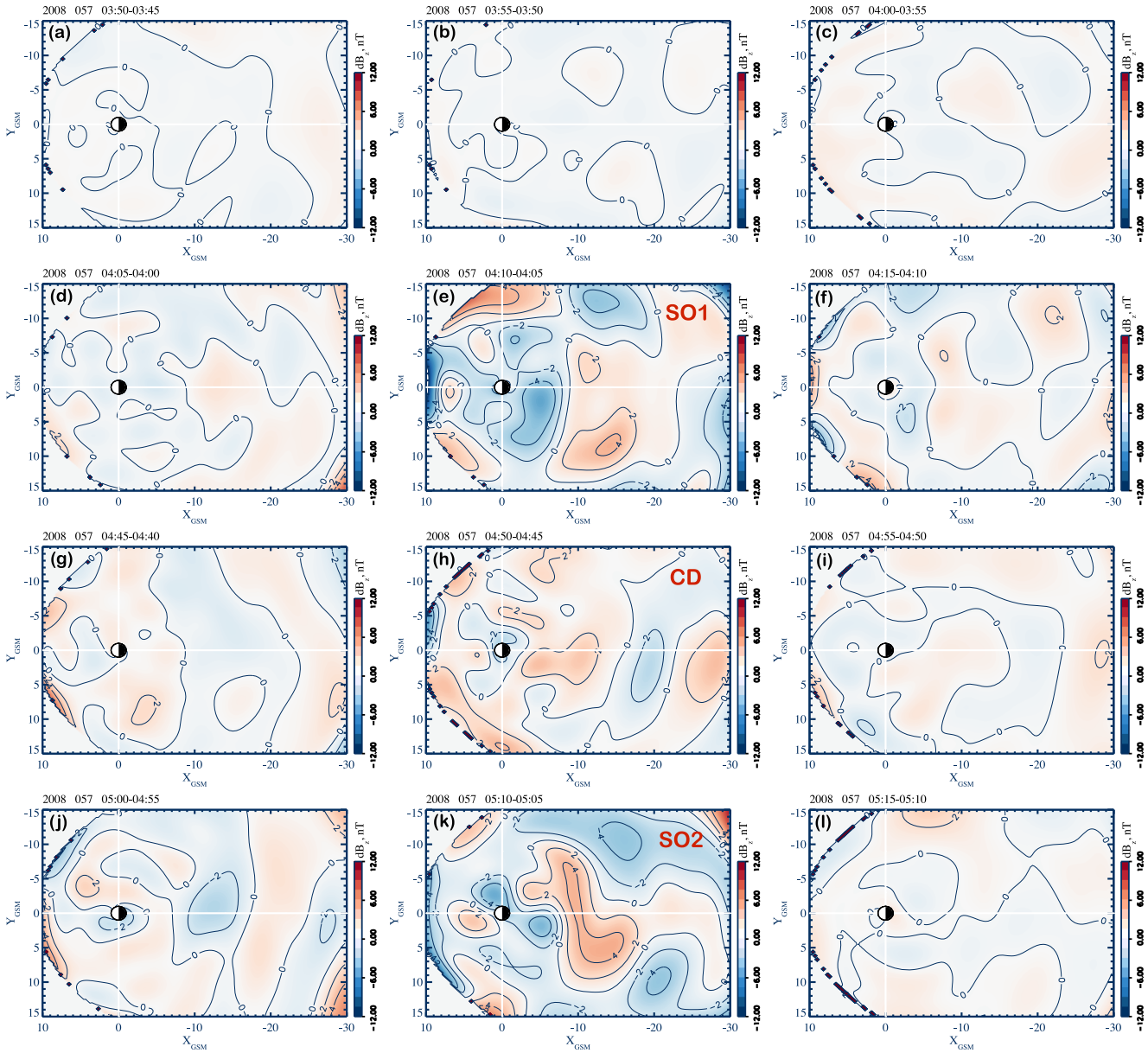

Figure 3. (a–l) The equatorial distributions of the magnetic field variations $dB_z = B_z(t_{i+1}) - B_z(t_i)$ with $t_{i+1} - t_i = 5$ min, for different times t_i in the event under scrutiny.

with SO1, SO2 and CD. They are contrasted with the neighboring intervals and the particularly quiet initial growth phase (Figures 3a–3d) when $|dB_z| < 1$ nT.

Interestingly, during activations SO1 and SO2 associated with MR, reflected in indices and discussed in the context of local THEMIS observations (Angelopoulos et al., 2008, 2009; Pu et al., 2010), the flux increases in the range ($-18\,R_E < x < -8\,R_E$), based on the 2 nT B_z increase threshold, with the peaks at $y \sim 10\,R_E$ and $y \sim 5\,R_E$ for SO1 and SO2 onsets, respectively. In contrast, the flux increase at the CD onset takes place in the radial range $4\,R_E < r < 12\,R_E$ with the peak at $y \sim 2\,R_E$ (although there is also a noticeable flux increase farther in the tail between 25 and 30 R_E). This difference suggests that the decay of the near-Earth current was indeed associated with processes closer to the Earth and to the midnight meridian, and it might not be directly connected with reconnection beyond 20 R_E. Figure 3 also suggests that both CD and MR processes describe different aspects of the same global flux redistribution (earhward in the near-Earth tail) rather than competing alternatives of the substorm tail

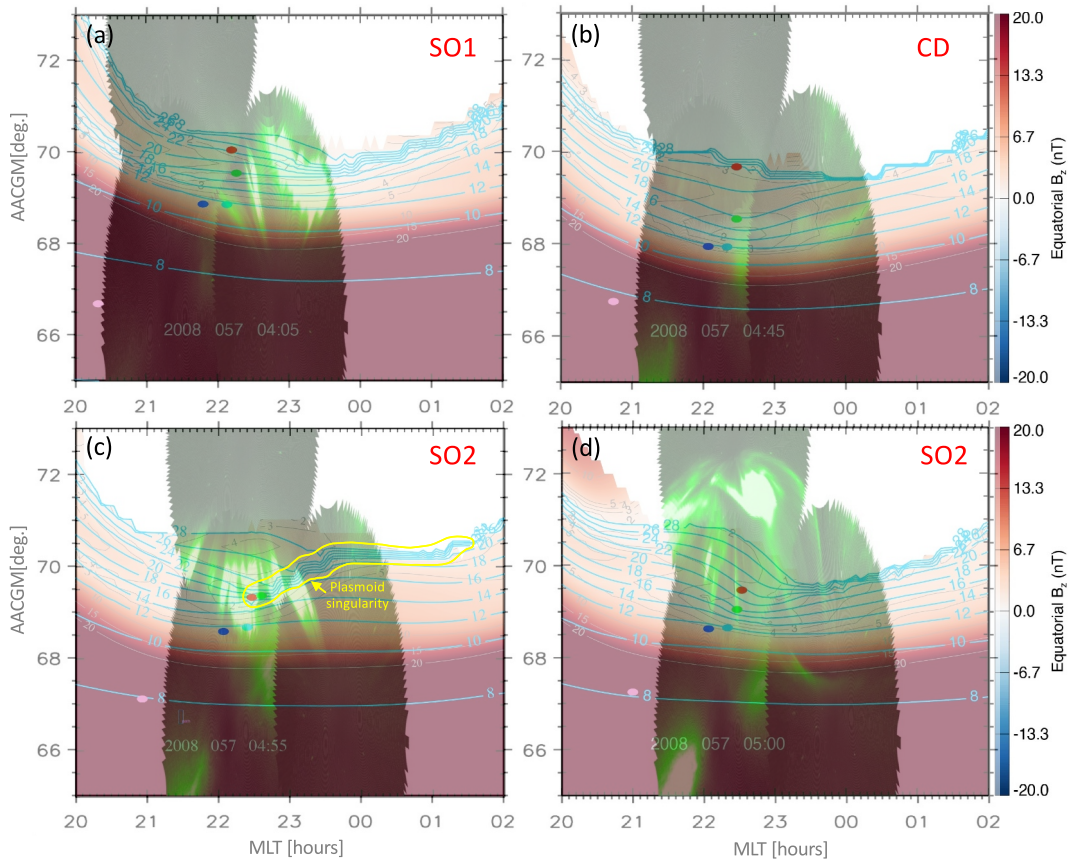

Figure 4. The all-sky imager (ASI) images (white-green shading) plotted with 50% transparency over the equatorial color-coded (blue-red) distributions of the magnetic field B_z for SO1, SO2, and CD onsets mapped to the low-altitude (MLT, AACGM) grid. The iso-contours of the B_z field and the radial distance are shown by gray and blue lines. The yellow contour in panel (c) marks the vicinity of the plasmoid seen in Figure 1b. The footpoints of the probes P1–P5 are color coded consistent with Figure 1. The original ASI images and low-altitude B_z maps are provided in Figures S6 and S7 in Supporting Information S1.

evolution. They all are skewed to the premidnight sector, consistent with previous statistical studies of substorm onsets based on IMAGE-FUV data (Frey et al., 2004).

5. Low-Altitude Maps and Their Comparison With ASI Pictures

To further investigate the mechanisms and possible triggers of the flux redistribution events, SO1, SO2 and CD, we mapped the corresponding distributions to low altitudes on the MLat-MLT plane in AACGM coordinates (AACGM is the Altitude-Adjusted Corrected Geomagnetic coordinate system (Shepherd, 2014)) and compared them with the corresponding instantaneous images taken by the THEMIS ASIs with 3-s cadence (Mende et al., 2008).

The results are presented in Figure 4, where instantaneous snapshots of ASI data selected at the same time stamps as the DM results are plotted translucently over the corresponding B_z distribution on (MLT, AACGM) plane. (Full ASI animations for the period 03:30:00–05:30:00 UT are provided in Movies S1 and S2.) It shows, first of all, that since plasmoids with their closed field line loops cannot be mapped to low altitudes, they appear in the (MLT, AACGM) plane as the regions of bunching of the radial distance iso-contours. Such a plasmoid singularity near the $B_z = 0$ loop in the tail shown in Figure 1b is marked by a yellow contour in Figure 4c. Note here that ARGUS provides a detailed reconstruction of FACs, making it possible, in particular, to describe the 3-D structure of the substorm current wedge (Stephens et al., 2019, Figure 10) and taking into account mapping distortions caused by field-line potential drops and resulting FACs.

Figure 4a suggests that the source of SO1 is in the premidnight sector and it is likely the X-line, which is seen beyond 24 R_E in Figure 2e. In contrast, the auroral activity at the CD onset, according to Figure 4b, has a source in the near-Earth tail close to the midnight meridian at radial distances 12–14 R_E. This location matches the region of the peak current density in Figure 2b, whose decay is seen in Figure S3f in Supporting Information S1 (orange line), 2c, 2k and Figure S4 in Supporting Information S1. Animation AS2 shows that wavy ray structures along the arc seen in Figure 4b brighten between 04:37 and 04:45 UT near the CD footprint and then decay. These features are consistent with the CD theory (Lui, 1996, 2016a; Lui et al., 1990). It includes the auroral brightening caused by thin and intense current sheets and their current- and buoyancy-driven instabilities, which ends around 04:45 UT when the current is disrupted and the equatorial field B_z is dipolarized (blue line in Figure S3g in Supporting Information S1). Note that in a number of aspects (lack of ionospheric closure shown in Figure S4 in Supporting Information S1; ASI image evolution similar to (Fukui et al., 2020, Figure 1)), the CD onset resembles pseudobreakups/pseudosubstorms. This CD activity could likely be missed by THEMIS probes because its peak, seen in Figure 4b, was shifted in MLT relative to THEMIS (the bright spot near 22:30 MLT is likely a moonlight/cloud effect).

As is seen from Figure 4c, some activity during SO2 may be rooted in the plasmoid shown in Figure 1b whose X-line protrusion between P1 and P2 is consistent with AN08. However, this activity is mainly in the premidnight sector and its source should be located beyond 28 R_E (the farthest radial distance iso-contour). This conclusion is further supported by Figure 4d, which shows strong activity way beyond 28 R_E. These features are consistent with indications of the persistent reconnection processes at or beyond 30 R_E (Imber et al., 2011; Zhao et al., 2016) based on the statistical studies of traveling compression regions, transient variations of the lobe magnetic field considered a remote effect of the plasmoid/flux rope passages (Slavin et al., 1984). They are also consistent with the concept of the new plasma intrusion from the open/closed boundary triggering activity in the near-Earth tail via fast plasma flows linked to north–south auroras proposed on the basis of extensive analysis of the substorm-time ASI observations (Nishimura et al., 2010) and correlated plasma observations in the tail (Nishimura et al., 2013).

6. Conclusions

The modern geomagnetic field reconstruction algorithm, based on DM (Sitnov et al., 2008; Stephens et al., 2019; Stephens & Sitnov, 2021) and ARGUS architecture (Stephens et al., 2024), resolves the X-line identified by in situ THEMIS observations (Angelopoulos et al., 2008). Moreover, it suggests that the discovered X-line is a generic feature of the specific state of the magnetosphere determined by its global input and state parameters, such as the geomagnetic indices and their time derivatives. The corresponding global magnetic field distribution is reconstructed on the basis of ∼26,000 virtual spacecraft from the history of substorm observations since 1995 shown in Figure 1.

The DM reconstructions also resolve other X-lines before and after the 04:55–05:00 UT onset, which might be missed by THEMIS probes located in the pre-midnight sector. Furthermore, the CD is also detected near the midnight meridian between substorm activations SO1 and SO2 in this event. It might also be missed by THEMIS probes as is seen from the comparison of the low-altitude maps of the equatorial magnetic field B_z with all-sky images.

In the presented DM picture, the most prominent feature of both substorm onsets occurred at 04:05 and 04:55 UT as well as the CD onset at 04:45 is the rapid redistribution of the magnetic flux in the premidnight sector (Figure 3). Both "classic reconnection onsets" (aka magnetic topology changes) and the CD (an abrupt reduction of the intense and thin current) appear as just different manifestations/aspects of this general flux redistribution process. This is consistent with recent interpretation of substorm mechanisms based on ballooning/interchange (Lui, 2016b; Merkin & Sitnov, 2016; Pritchett & Coroniti, 2013) and tearing/magnetic flux release (Birn et al., 2018; Merkin et al., 2015; Sitnov et al., 2014; Sitnov, Stephens, et al., 2021) instabilities, their small-scale manifestations in the form of dipolarization fronts (Runov et al., 2009; Sitnov et al., 2009) and plasma watersheds (Motoba et al., 2022; Sitnov, Motoba, & Swisdak, 2021), as well as global scenarios, such as the slingshot relaxation mechanism proposed by Machida et al. (2009) based on their statistical visualization of the magnetotail around substorm onsets.

Finally, the DM technology provides a more accurate and detailed description of substorms at low altitudes compared to earlier empirical models (cf. Figure 2g in AN08), including the resolution of plasmoid (Figure 4c) and CD regions (Figure 4b). Its comparison with ASI data suggests that these rapid reconfigurations of the

magnetotail may be triggered by plasma flows whose source is farther from Earth than the resolved X-lines (Nishimura et al., 2010, 2013). It also suggests that the CD may have a local activation mechanism associated with the plasma instabilities in the transition region between the tail and the inner magnetosphere.

Conflict of Interest

The authors declare no conflicts of interest relevant to this study.

Data Availability Statement

The data used in the paper are archived on Zenodo (Sitnov, Stephens, Motoba, & Tsyganenko, 2025). The ASI images has been retrieved from the THEMIS ASI GBO data reader (https://themis.ssl.berkeley.edu/data/themis/thg/).

Acknowledgments
The authors acknowledge useful discussions with V. Angelopoulos, A. V. Artemyev and A. T. Y. Lui. They thank the SuperMag team and their collaborators, which provided the global indices of the storm and substorm activity. They also thank the teams who provided Geotail, Polar, IMP 8, Cluster, THEMIS, Van Allen Probes, MMS and GOES data obtained via NSSDC CDAWeb online facility, as well as Wind and ACE solar wind/IMF data that went into the production of the OMNI data obtained via NASA/GSFC's Space Physics Data Facility's OMNIWeb service. The 3-D visualizations were performed using VisIt, which is supported by the Department of Energy with funding from the Advanced Simulation and Computing Program and the Scientific Discovery through Advanced Computing Program. This work was funded by NASA Grants 80NSSC20K1271, 80NSSC24K0268, 80NSSC24K0556, 80NSSC25K 0073, 80NSSC25K0076, and 80NSSC 25K7676, as well as the NSF Grant AGS-2411808.

References

Aggarwal, C. C. (2014). Instance-based learning: A survey. In C. C. Aggarwal (Ed.), *Data classification* (pp. 157–185). Chapman and Hall/CRC.
Alken, P., Thébault, E., Beggan, C. D., Amit, H., Aubert, J., Baerenzung, J., et al. (2021). International geomagnetic reference field: The thirteenth generation. *Earth Planets and Space*, *73*(1), 49. https://doi.org/10.1186/s40623-020-01288-x
Angelopoulos, V. (2008). The THEMIS mission. *Space Science Reviews*, *141*(1), 5–34. https://doi.org/10.1007/s11214-008-9336-1
Angelopoulos, V., McFadden, J. P., Larson, D., Carlson, C. W., Mende, S. B., Frey, H., et al. (2008). Tail reconnection triggering substorm onset. *Science*, *321*(5891), 931–935. https://doi.org/10.1126/science.1160495
Angelopoulos, V., McFadden, J. P., Larson, D., Carlson, C. W., Mende, S. B., Frey, H., et al. (2009). Response to comment on "Tail reconnection triggering substorm onset". *Science*, *324*(5933), 1391. https://doi.org/10.1126/science.1168045
Angelopoulos, V., Runov, A., Zhou, X.-Z., Turner, D. L., Kiehas, S. A., Li, S.-S., & Shinohara, I. (2013). Electromagnetic energy conversion at reconnection fronts. *Science*, *341*(6153), 1478–1482. https://doi.org/10.1126/science.1236992
Baker, D. N., Pulkkinen, T. I., Angelopoulos, V., Baumjohann, W., & McPherron, R. L. (1996). Neutral line model of substorms: Past results and present view. *Journal of Geophysical Research*, *101*(A6), 12975–13010. https://doi.org/10.1029/95JA03753
Birn, J., Merkin, V. G., Sitnov, M. I., & Otto, A. (2018). MHD stability of magnetotail configurations with a Bz hump. *Journal of Geophysical Research: Space Physics*, *123*(5), 3477–3492. https://doi.org/10.1029/2018JA025290
Burton, R. K., McPherron, R. L., & Russell, C. T. (1975). An empirical relationship between interplanetary conditions and Dst. *Journal of Geophysical Research (1896-1977)*, *80*(31), 4204–4214. https://doi.org/10.1029/JA080i031p04204
Coppi, B., Laval, G., & Pellat, R. (1966). Dynamics of the geomagnetic tail. *Physical Review Letters*, *16*(26), 1207–1210. https://doi.org/10.1103/PhysRevLett.16.1207
Cover, T., & Hart, P. (1967). Nearest neighbor pattern classification. *IEEE Transactions on Information Theory*, *13*(1), 21–27. https://doi.org/10.1109/TIT.1967.1053964
Crooker, N. U., & McPherron, R. L. (1972). On the distinction between the auroral electrojet and partial ring current systems. *Journal of Geophysical Research (1896-1977)*, *77*(34), 6886–6889. https://doi.org/10.1029/JA077i034p06886
Dou, B., Zhu, Z., Merkurjev, E., Ke, L., Chen, L., Jiang, J., et al. (2023). Machine learning methods for small data challenges in molecular science. *Chemical Reviews*, *123*(13), 8736–8780. https://doi.org/10.1021/acs.chemrev.3c00189
Farmer, J. D., & Sidorowich, J. J. (1987). Predicting chaotic time series. *Physical Review Letters*, *59*(8), 845–848. https://doi.org/10.1103/PhysRevLett.59.845
Frey, H. U., Mende, S. B., Angelopoulos, V., & Donovan, E. F. (2004). Substorm onset observations by IMAGE-FUV. *Journal of Geophysical Research*, *109*(A10), A10304. https://doi.org/10.1029/2004JA010607
Fukui, K., Miyashita, Y., Machida, S., Miyoshi, Y., Ieda, A., Nishimura, Y., & Angelopoulos, V. (2020). A statistical study of near-earth magnetotail evolution during pseudosubstorms and substorms with THEMIS data. *Journal of Geophysical Research: Space Physics*, *125*(1), e2019JA026642. https://doi.org/10.1029/2019JA026642
Gjerloev, J. W. (2012). The SuperMag data processing technique. *Journal of Geophysical Research*, *117*(A9), A09213. https://doi.org/10.1029/2012JA017683
Imber, S. M., Slavin, J. A., Auster, H. U., & Angelopoulos, V. (2011). A THEMIS survey of flux ropes and traveling compression regions: Location of the near-earth reconnection site during solar minimum. *Journal of Geophysical Research*, *116*(A2), A02201. https://doi.org/10.1029/2010JA016026
Jackson, D. D. (1972). Interpretation of inaccurate, insufficient and inconsistent data. *Geophysical Journal International*, *28*(2), 97–109. https://doi.org/10.1111/j.1365-246X.1972.tb06115.x
Kubyshkina, M., Sergeev, V., Tsyganenko, N., Angelopoulos, V., Runov, A., Singer, H., et al. (2009). Toward adapted time-dependent magnetospheric models: A simple approach based on tuning the standard model. *Journal of Geophysical Research*, *114*(A1), A00C21. https://doi.org/10.1029/2008JA013547
Lui, A. T. Y. (1996). Current disruption in the Earth's magnetosphere: Observations and models. *Journal of Geophysical Research*, *101*(A6), 13067–13088. https://doi.org/10.1029/96JA00079
Lui, A. T. Y. (2009). Comment on "Tail reconnection triggering substorm onset". *Science*, *324*(5933), 1391. https://doi.org/10.1126/science.1167726
Lui, A. T. Y. (2016a). Cross-field current instability for auroral bead formation in breakup arcs. *Geophysical Research Letters*, *43*(12), 6087–6095. https://doi.org/10.1002/2016GL069892
Lui, A. T. Y. (2016b). Dipolarization front and current disruption. *Geophysical Research Letters*, *43*(19), 10050–10058. https://doi.org/10.1002/2016GL070980
Lui, A. T. Y. (2020). Evaluation of the cross-field current instability as a substorm onset process with auroral bead properties. *Journal of Geophysical Research: Space Physics*, *125*(10), e2020JA027867. https://doi.org/10.1029/2020JA027867

Lui, A. T. Y., Mankofsky, A., Chang, C.-L., Papadopoulos, K., & Wu, C. S. (1990). A current disruption mechanism in the neutral sheet: A possible trigger for substorm expansions. *Geophysical Research Letters*, *17*(6), 745–748. https://doi.org/10.1029/GL017i006p00745

Machida, S., Miyashita, Y., Ieda, A., Nosé, M., Nagata, D., Liou, K., et al. (2009). Statistical visualization of the Earth's magnetotail based on Geotail data and the implied substorm model. *Annales Geophysicae*, *27*(3), 1035–1046. https://doi.org/10.5194/angeo-27-1035-2009

McPherron, R. L., Russell, C. T., & Aubry, M. P. (1973). Satellite studies of magnetospheric substorms on August 15, 1968: 9. Phenomenological model for substorms. *Journal of Geophysical Research*, *78*(16), 3131–3149. https://doi.org/10.1029/ja078i016p03131

Mende, S. B., Harris, S. E., Frey, H. U., Angelopoulos, V., Russell, C. T., Donovan, E., et al. (2008). The THEMIS array of ground-based observatories for the study of auroral substorms. *Space Science Reviews*, *141*(1), 357–387. https://doi.org/10.1007/s11214-008-9380-x

Merkin, V. G., & Sitnov, M. I. (2016). Stability of magnetotail equilibria with a tailward Bz gradient. *Journal of Geophysical Research: Space Physics*, *121*(10), 9411–9426. https://doi.org/10.1002/2016JA023005

Merkin, V. G., Sitnov, M. I., & Lyon, J. G. (2015). Evolution of generalized two-dimensional magnetotail equilibria in ideal and resistive MHD. *Journal of Geophysical Research: Space Physics*, *120*(3), 1993–2014. https://doi.org/10.1002/2014JA020651

Motoba, T., Sitnov, M. I., Stephens, G. K., & Gershman, D. J. (2022). A new perspective on magnetotail electron and ion divergent flows: MMS observations. *Journal of Geophysical Research: Space Physics*, *127*(10), e2022JA030514. https://doi.org/10.1029/2022JA030514

Nelder, J. A., & Mead, R. (1965). A simplex method for function minimization. *The Computer Journal*, *7*(4), 308–313. https://doi.org/10.1093/comjnl/7.4.308

Nishimura, Y., Bortnik, J., Li, W., Thorne, R. M., Lyons, L. R., Angelopoulos, V., et al. (2011). Estimation of magnetic field mapping accuracy using the pulsating aurora-chorus connection. *Geophysical Research Letters*, *38*(14), L14110. https://doi.org/10.1029/2011GL048281

Nishimura, Y., Lyons, L., Zou, S., Angelopoulos, V., & Mende, S. (2010). Substorm triggering by new plasma intrusion: THEMIS all-sky imager observations. *Journal of Geophysical Research*, *115*(A7), A07222. https://doi.org/10.1029/2009JA015166

Nishimura, Y., Lyons, L. R., Xing, X., Angelopoulos, V., Donovan, E. F., Mende, S. B., et al. (2013). Tail reconnection region versus auroral activity inferred from conjugate ARTEMIS plasma sheet flow and auroral observations. *Journal of Geophysical Research: Space Physics*, *118*(9), 5758–5766. https://doi.org/10.1002/jgra.50549

Partamies, N., Juusola, L., Tanskanen, E., & Kauristie, K. (2013). Statistical properties of substorms during different storm and solar cycle phases. *Annales Geophysicae*, *31*(2), 349–358. https://doi.org/10.5194/angeo-31-349-2013

Press, W. H., Teukolsky, S. A., Flannery, B. P., & Vetterling, W. T. (1992). *Numerical recipes in fortran: The art of scientific computing* (2nd ed.). Cambridge University Press.

Pritchett, P. L., & Coroniti, F. V. (2013). Structure and consequences of the kinetic ballooning/interchange instability in the magnetotail. *Journal of Geophysical Research: Space Physics*, *118*(1), 146–159. https://doi.org/10.1029/2012JA018143

Pu, Z. Y., Chu, X. N., Cao, X., Mishin, V., Angelopoulos, V., Wang, J., et al. (2010).THEMIS observations of substorms on 26 February 2008 initiated by magnetotail reconnection. *Journal of Geophysical Research*, *115*(A2), A02212. https://doi.org/10.1029/2009JA014217

Runov, A., Angelopoulos, V., Sitnov, M. I., Sergeev, V. A., Bonnell, J., McFadden, J. P., et al. (2009). THEMIS observations of an earthward-propagating dipolarization front. *Geophysical Research Letters*, *36*(14), L14106. https://doi.org/10.1029/2009GL038980

Runov, A., Sergeev, V. A., Baumjohann, W., Nakamura, R., Apatenkov, S., Asano, Y., et al. (2005). Electric current and magnetic field geometry in flapping magnetotail current sheets. *Annales Geophysicae*, *23*(4), 1391–1403. https://doi.org/10.5194/angeo-23-1391-2005

Schindler, K. (1974). A theory of the substorm mechanism. *Journal of Geophysical Research*, *79*(19), 2803–2810. https://doi.org/10.1029/JA079i019p02803

Sergeev, V., Nishimura, Y., Kubyshkina, M., Angelopoulos, V., Nakamura, R., & Singer, H. (2012). Magnetospheric location of the equatorward prebreakup arc. *Journal of Geophysical Research*, *117*(A1), A01212. https://doi.org/10.1029/2011JA017154

Sergeev, V. A., Angelopoulos, V., Kubyshkina, M., Donovan, E., Zhou, X.-Z., Runov, A., et al. (2011). Substorm growth and expansion onset as observed with ideal ground-spacecraft THEMIS coverage. *Journal of Geophysical Research*, *116*(A5), A00I26. https://doi.org/10.1029/2010JA015689

Shepherd, S. G. (2014). Altitude-adjusted corrected geomagnetic coordinates: Definition and functional approximations. *Journal of Geophysical Research: Space Physics*, *119*(9), 7501–7521. https://doi.org/10.1002/2014JA020264

Shevchenko, I. G., Sergeev, V., Kubyshkina, M., Angelopoulos, V., Glassmeier, K. H., & Singer, H. J. (2010). Estimation of magnetosphere-ionosphere mapping accuracy using isotropy boundary and THEMIS observations. *Journal of Geophysical Research*, *115*(A11), A11206. https://doi.org/10.1029/2010JA015354

Shi, X., Stephens, G. K., Artemyev, A. V., Sitnov, M. I., & Angelopoulos, V. (2024). Picturing global substorm dynamics in the magnetotail using low-altitude ELFIN measurements and data mining-based magnetic field reconstructions. *Space Weather*, *22*(10), e2024SW004062. https://doi.org/10.1029/2024SW004062

Sitnov, M. I., Merkin, V. G., Swisdak, M., Motoba, T., Buzulukova, N., Moore, T. E., et al. (2014). Magnetic reconnection, buoyancy, and flapping motions in magnetotail explosions. *Journal of Geophysical Research: Space Physics*, *119*(9), 7151–7168. https://doi.org/10.1002/2014JA020205

Sitnov, M. I., Motoba, T., & Swisdak, M. (2021). Multiscale nature of the magnetotail reconnection onset. *Geophysical Research Letters*, *48*(10), e2021GL093065. https://doi.org/10.1029/2021GL093065

Sitnov, M. I., Stephens, G. K., Artemyev, A. V., Motoba, T., & Tsyganenko, N. A. (2025). Global structure of the cislunar magnetotail and its evolution during substorms. *Journal of Geophysical Research: Space Physics*, *130*(7), e2025JA034018. https://doi.org/10.1029/2025JA034018

Sitnov, M. I., Stephens, G. K., Motoba, T., & Swisdak, M. (2021). Data mining reconstruction of magnetotail reconnection and implications for its first-principle modeling. *Frontiers in Physics*, *9*, 644884. https://doi.org/10.3389/fphy.2021.644884

Sitnov, M. I., Stephens, G. K., Motoba, T., & Tsyganenko, N. (2025). The 26 February 2008 substorms: Data-mining picture [dataset]. *Zenodo*. https://doi.org/10.5281/zenodo.15313955

Sitnov, M. I., Stephens, G. K., Tsyganenko, N. A., Miyashita, Y., Merkin, V. G., Motoba, T., et al. (2019). Signatures of nonideal plasma evolution during substorms obtained by mining multimission magnetometer data. *Journal of Geophysical Research: Space Physics*, *124*(11), 8427–8456. https://doi.org/10.1029/2019JA027037

Sitnov, M. I., Stephens, G. K., Tsyganenko, N. A., Ukhorskiy, A. Y., Wing, S., Korth, H., & Anderson, B. J. (2017). Spatial structure and asymmetries of magnetospheric currents inferred from high-resolution empirical geomagnetic field models. In *Dawn-dusk asymmetries in planetary plasma environments* (pp. 199–212). American Geophysical Union (AGU). https://doi.org/10.1002/9781119216346.ch15

Sitnov, M. I., Swisdak, M., & Divin, A. V. (2009). Dipolarization fronts as a signature of transient reconnection in the magnetotail. *Journal of Geophysical Research*, *114*(A4), A04202. https://doi.org/10.1029/2008JA013980

Sitnov, M. I., Tsyganenko, N. A., Ukhorskiy, A. Y., & Brandt, P. C. (2008). Dynamical data-based modeling of the storm-time geomagnetic field with enhanced spatial resolution. *Journal of Geophysical Research*, *113*(A7), A07218. https://doi.org/10.1029/2007JA013003

Slavin, J. A., Smith, E. J., Tsurutani, B. T., Sibeck, D. G., Singer, H. J., Baker, D. N., et al. (1984). Substorm associated traveling compression regions in the distant tail: Isee-3 Geotail observations. *Geophysical Research Letters*, *11*(7), 657–660. https://doi.org/10.1029/GL011i007p00657

Speiser, T. W. (1965). Particle trajectories in model current sheets: 1. Analytical solutions. *Journal of Geophysical Research (1896-1977)*, *70*(17), 4219–4226. https://doi.org/10.1029/JZ070i017p04219

Stephens, G. K., Bingham, S. T., Sitnov, M. I., Gkioulidou, M., Merkin, V. G., Korth, H., et al. (2020). Storm time plasma pressure inferred from multimission measurements and its validation using Van Allen Probes particle data. *Space Weather*, *18*(12), e2020SW002583. https://doi.org/10.1029/2020SW002583

Stephens, G. K., & Sitnov, M. I. (2021). Concurrent empirical magnetic reconstruction of storm and substorm spatial scales using data mining and virtual spacecraft. *Frontiers in Physics*, *9*, 210. https://doi.org/10.3389/fphy.2021.653111

Stephens, G. K., Sitnov, M. I., Korth, H., Tsyganenko, N. A., Ohtani, S., Gkioulidou, M., & Ukhorskiy, A. Y. (2019). Global empirical picture of magnetospheric substorms inferred from multimission magnetometer data. *Journal of Geophysical Research: Space Physics*, *124*(2), 1085–1110. https://doi.org/10.1029/2018JA025843

Stephens, G. K., Sitnov, M. I., & Tsyganenko, N. A. (2024). AI-based reconstruction of the geospace unified system. Retrieved from https://github.com/grantkstephens/ARGUS

Stephens, G. K., Sitnov, M. I., Ukhorskiy, A. Y., Roelof, E. C., Tsyganenko, N. A., & Le, G. (2016). Empirical modeling of the storm time innermost magnetosphere using Van Allen probes and THEMIS data: Eastward and banana currents. *Journal of Geophysical Research: Space Physics*, *121*(1), 157–170. https://doi.org/10.1002/2015JA021700

Stephens, G. K., Sitnov, M. I., Weigel, R. S., Turner, D. L., Tsyganenko, N. A., Rogers, A. J., et al. (2023). Global structure of magnetotail reconnection revealed by mining space magnetometer data. *Journal of Geophysical Research: Space Physics*, *128*(2), e2022JA031066. https://doi.org/10.1029/2022JA031066

Sun, B., & Chen, H. (2021). A survey of k nearest neighbor algorithms for solving the class imbalanced problem. *Wireless Communications and Mobile Computing*, *2021*(1), 5520990. https://doi.org/10.1155/2021/5520990

Tsyganenko, N. A. (1995). Modeling the Earth's magnetospheric magnetic field confined within a realistic magnetopause. *Journal of Geophysical Research*, *100*(A4), 5599–5612. https://doi.org/10.1029/94JA03193

Tsyganenko, N. A. (1996). Effects of the solar wind conditions on the global magnetospheric configurations as deduced from data-based field models. In *Proceedings of the third international conference on substorms (ICS-3)* (pp. 181–185).

Tsyganenko, N. A. (2002). A model of the near magnetosphere with a dawn-dusk asymmetry 1. Mathematical structure. *Journal of Geophysical Research*, *107*(A8), SMP12-1–15. https://doi.org/10.1029/2001JA000219

Tsyganenko, N. A., & Andreeva, V. A. (2014). On the "bowl-shaped" deformation of planetary equatorial current sheets. *Geophysical Research Letters*, *41*(4), 1079–1084. https://doi.org/10.1002/2014GL059295

Tsyganenko, N. A., Andreeva, V. A., Sitnov, M. I., Stephens, G. K., Gjerloev, J. W., Chu, X., & Troshichev, O. A. (2021). Reconstructing substorms via historical data mining: Is it really feasible? *Journal of Geophysical Research: Space Physics*, *126*(10), e2021JA029604. https://doi.org/10.1029/2021JA029604

Tsyganenko, N. A., & Sitnov, M. I. (2007). Magnetospheric configurations from a high-resolution data-based magnetic field model. *Journal of Geophysical Research*, *112*(A6), A06225. https://doi.org/10.1029/2007JA012260

Tsyganenko, N. A., & Stern, D. P. (1996). Modeling the global magnetic field of the large-scale Birkeland current systems. *Journal of Geophysical Research*, *101*(A12), 27187–27198. https://doi.org/10.1029/96JA02735

Turner, D. L., Fennell, J. F., Blake, J. B., Claudepierre, S. G., Clemmons, J. H., Jaynes, A. N., et al. (2017). Multipoint observations of energetic particle injections and substorm activity during a conjunction between Magnetospheric Multiscale (MMS) and Van Allen Probes. *Journal of Geophysical Research: Space Physics*, *122*(11), 11481–11504. https://doi.org/10.1002/2017JA024554

Vassiliadis, D. (2006). Systems theory for geospace plasma dynamics. *Reviews of Geophysics*, *44*(2), RG2002. https://doi.org/10.1029/2004RG000161

Vassiliadis, D., Klimas, A. J., Baker, D. N., & Roberts, D. A. (1995). A description of the solar wind-magnetosphere coupling based on nonlinear filters. *Journal of Geophysical Research*, *100*(A3), 3495–3512. https://doi.org/10.1029/94JA02725

Zhao, S., Tian, A., Shi, Q., Xiao, C., Fu, S., Zong, Q., et al. (2016). Statistical study of magnetotail flux ropes near the lunar orbit. *Science China Technological Sciences*, *59*(10), 1591–1596. https://doi.org/10.1007/s11431-015-0962-3